Phagocytosis of Polymeric Nanoparticles Aided Activation of Macrophages to Induce Atherosclerotic Plaques in Apoe$^{-/-}$ Mice

Tieying Yin (tieying_yin@cqu.edu.cn)
Key Laboratory for Biorheological Science and Technology of Ministry of Education, State and Local Joint Engineering Laboratory for Vascular Implants, Bioengineering College of Chongqing University, Chongqing, 400044, China https://orcid.org/0000-0002-0424-776X

Yanhong Li
Chongqing University

Rohmana Maftuhatul Fuad Atik
Chongqing University

Yuzhen Ren
Chongqing University

Fangfang Hu
Chongqing University

Ruolin Du
Chongqing University

Yang Wang
Chongqing University

Guixue Wang
Chongqing University

Yazhou Wang
Chongqing University of Medical Science: Chongqing Medical University

Research

Keywords: Nanomedicine, Atherosclerosis, Macrophages, Phagocytosis, Foam cell

Posted Date: December 18th, 2020

DOI: https://doi.org/10.21203/rs.3.rs-128665/v1

Abstract

The unique physiochemical properties of nanomaterials have been widely used in drug delivery systems and diagnostic contrast agents. The safety issues of biomaterials with exceptional biocompatibility and hemo-compatibility have also received extensive attention at the nanoscale, especially in cardiovascular disease. Therefore, we conducted a study of the effects of poly (lactic-co-glycolic acid) nanoparticles (PLGA NPs) on the development of aortic atherosclerotic plaques in $ApoE^{-/-}$ mice. The particle size of PLGA NPs was 92.69 ± 3.1 nm and the zeta potential were -31.6 ± 2.8 mV, with good blood compatibility. $ApoE^{-/-}$ mice were continuously injected with PLGA NPs intravenously for 4 and 12 weeks. Examination of oil red O stained aortic sinuses confirmed that the accumulation of PLGA NPs promoted the formation of atherosclerotic plaques and increasing the expression of associated inflammatory factors, such as TNF-α, IL-6, and IL-10. The combined exposure of ox-LDL and PLGA NPs accelerated the conversion of macrophages to foam cells. Our results highlight the potential risk for PLGA NPs *in vivo* and further understanding the interaction between PLGA NPs and the atherosclerotic plaques, which we should consider in future nanomaterial design and pay more attention to the process of using nano-medicines on cardiovascular diseases.

1. Introduction

Nanoparticles are ultrafine particles with at least one dimension < 100 nm in size. Nanoparticles possess physical properties, such as macroscopic quantum tunneling, nano size and surface effects, which make them desirable for applications in medicine, materials science and biology [1, 2]. Nanoparticles may accumulate within the human body through inhalation, ingestion, skin absorption, and injection [3, 4]. The biological safety of nanomaterials has received widespread attention due to their special properties including small size and high specific surface area [5]. An accumulation of nanoparticles in the lungs will result in passage through the alveolar epithelial cells or lymphatic system into the circulation to be redistributed throughout the body. Therefore, nanoparticles may have a significant impact on the cardiovascular system [6, 7, 8]. Studies have shown that atmospheric particulate matter (PM), composed mainly of nanoparticles, increases cardiovascular disease morbidity and mortality. The cardiovascular system is now recognized as one of the important targets of nano-toxicity [9, 10].

Nanoparticles have more serious biological toxicity and more complex toxicological mechanisms than common chemicals. Studies have shown that nanoparticles can damage vascular endothelial cells and trigger an inflammatory reaction, which in turn may cause platelet aggregation and thrombosis [11, 12, 13]. Therefore, nanoparticles may be an important risk factor for cardiovascular diseases such as atherosclerosis (AS) [14, 15, 16]. Medical research has shown that an inflammatory response is an important pathological mechanism for the development of AS, which can cause endothelial cell dysfunction. When nanoparticles adhere to the cell membrane of endothelial cells, they induce the expression and release of inflammatory factors (such as IL-6, IL-8, and TNF-α) [17, 18]. Nanoparticles also may promote adhesion of monocytes to endothelial cells, further differentiation into macrophages, and

penetration of the blood vessel walls, leading to AS [19]. Accumulating lipids in unstable plaques further exacerbate the inflammatory response, thereby promoting the development of AS [20]. Nanoparticles induce inflammatory reactions, impair lysosomal function, promote abnormal hydrolysis of triglycerides, and lead to an increased lipid load in macrophages, which in turn induces foam cell formation. In the inflammatory state, vascular smooth muscle cells, dendritic cells, and mast cells also may produce foam cells. Nanoparticles activate neutrophil elastase, which degrades elastin and various collagens, damaging vascular endothelial cells (VECs) and basement membranes [21]. Nanoparticles interacts with the complement system, coagulation functions and fibrinolysis, which aggravates the formation and instability of arterial plaque [22].

Pober and Cotran examined the relationship between AS and hemodynamics and proposed the shear stress theory to describe the onset of AS [23]. At present, it is well known that atherosclerotic lesions are mainly concentrated in sites with obvious changes in blood flow. In the early stage of plaque development, endothelial cells on the arterial wall attract monocytes, which transform into macrophages and then absorb large amounts of oxidized low-density lipoprotein (ox-LDL) to transform into foam cells. Therefore, atherosclerotic lesions are complex environments containing lipids, cholesterol crystals, inflammatory cells and secreted cytokines. However, when nanoparticles enter the body, they tend to accumulate in areas of infarction. Studies have found that nanoparticles with longer blood circulation times are more likely to cross the endothelial barrier and accumulate in the infarcted area due to the destruction of the endothelial barrier caused by ischemic injury. This mechanism is similar to enhanced permeability and retention [24, 25, 26].

In 2007, Dawson and Linse jointly proposed the concept of a protein corona, which led researchers to study the fate of nanoparticles *in vivo* [27]. Nanoparticles will rapidly adsorb proteins forming what is known as the protein “corona” after enters the circulation system. The structure and composition of the protein corona depends on the synthetic identity of the nanomaterial, this would influence the biological identity of nanoparticles [28]. The physiological functions of various proteins that comprise the protein corona generally involve lipid transport, coagulation, complement activation, pathogen recognition, or ion transport [29]. Understanding nanoparticle-protein interactions is a crucial issue in the development of targeted nanomaterial delivery *in vivo* [30]. The physiological environment to which nanoparticles are first exposed after intravenous administration is the blood stream, and the cell-free portion of the blood (plasma) contains more than 1000 proteins. These proteins potentially interact with nanoparticles to exert different physiological functions, such as recognition by macrophages, causing inflammatory reactions, thrombosis and allergic reactions [31].

The safety issues of biomaterials with exceptional biocompatibility and hemo-compatibility have also received extensive attention at the nanoscale. Numerous nanomaterials have been widely used as drug delivery systems and diagnostic contrast agents in treating cardiovascular diseases. This article focuses on polymer nanoparticles and explores their bioactivity impact on the development of AS and physiochemical mechanisms. Therefore, we conducted a study of the effects of poly (lactic-co-glycolic

acid) (PLGA) nanoparticles, which are widely used in a variety of Food and Drug Administration (FDA) approved therapeutic devices, on the development of aortic atherosclerotic plaques in ApoE$^{-/-}$ mice.

2. Methods Experimental Materials And Methods

2.1. Experimental materials

PLGA polymer (MW: 90000, 50:50), Eight-week-old C57 BL/6 and ApoE$^{-/-}$ male weighed 20–25 g mice were purchased from Beijing Weitong Lihua Experimental Animal Technology Co.Ltd. (Beijing, China). Male New Zealand white rabbit weighed 3 kg were purchased from Chongqing Daping Hospital Animal Experimental Center (Chongqing, China). The high fat diet contained 0.15% cholesterol and 20% fat. The murine macrophage cell line (Raw 264.7) was purchased from American Type Culture Collection (ATCC, USA).

2.2. Methods

2.2.1. Preparation of PLGA nanoparticles and PLGA + PC

PLGA nanoparticle were prepared by a nanoprecipitation proses [32]. Briefly, PLGA (100 mg) was dissolved into 10 mL dimethyl sulfoxide (DMSO). The mixture (2 mL) was precipitated by adding dropwise into 6 mL deionized water with gentle stirring, and further dialyzed using dialysis bag (molecular weight cut-off, MWCO: 3500 Da) against water to remove the free DMSO. The volume was adjusted to 10 mL to obtain PLGA nanoparticles solution (2 mg/mL), collected and preserved at 4 °C. The blood was collected with heparin from the eyeball and stored at 4 °C. The collected blood of the mice was statically placed at 4 ℃ and after 6 hours, centrifuged at 3000 rmp for 15 min to obtain serum. To obtain PLGA + protein corona (PC), 1 mL of solution of PLGA (2 mg/mL) was incubated with 5 μg of serum at 37 °C for 30 min.

2.2.2. Characterization of PLGA Nanoparticles and PLGA + PC

The aqueous phase diameter, size and zeta potential of PLGA nanoparticles and PLGA + PC were determined by dynamic light scattering (DLS) using a Malvern Zetasizer Nano ZS unit (Nano ZS 90, Malvern, UK) with He-Ne laser (λ = 633 nm) at a scattering angle of 90° at 25 °C. A drop of PLGA nanoparticles or PLGA + PC solution at a concentration of 100 μg/mL was dropped onto a copper mesh (200 mesh), and air-dried naturally. Then stained by 2% phosphotungstic acid for 3 min, air-drying. Subsequently, the morphology of PLGA nanoparticles and PLGA + PC were visually observed using a transmission electron microscope (TEM, Zeiss Germany, Optima 75 KV).

2.2.3. Determination of serum protein adsorbed by PLGA nanoparticles

Determination of serum protein adsorbed by PLGA nanoparticles was carried out according to the standards BCA protein assay kit. PLGA nanoparticles were incubated with 2 mL mouse serum for 30 min,

the mixture was centrifuged at 3000 rpm for 20 min, and then the supernatant was collected to determine protein content by the BCA kit. Meantime, untreated serum was the control group.

2.2.4. Hemolysis rate of PLGA nanoparticles

The collected fresh vein blood from healthy rabbits were mixed with sodium citrate in a 9:1 ratio to prevent coagulation. Four microliters anticoagulation was added with 5 mL 0.9% sodium chloride (NaCl) injection to dilute. The first group as a negative control contained 5% glucose, second group as a positive control contained only deionized water and the last group as experimental group consisting of three sub-groups, 2 mg/ml PLGA nanoparticles, 1 mg/mL PLGA nanoparticles and isotonic solution that contained a mixture of PLGA nanoparticles and 5% glucose.

Then, each group above solution (200 μL) was incubated with 0.9% NaCl (2.8 mL) at 37 °C for 30 min in a water bath. The mixture was added 60 μL of diluted anticoagulant solution, after second incubation at 37 °C for 60 min in a water bath and centrifugation 3000 rpm for 10 min, the supernatant was collected and measured absorbance (OD) at 545 nm spectrophotometer.

To quantify percent hemolysis, the hemoglobin concentration measured was divided by the hemoglobin concentration of the diluted blood solution as described by the following equation:

$$Hemolysis\ rate\ (\%) = \left(\frac{OD\ sample\ -OD\ negative\ control}{OD\ positive\ control-OD\ negative\ control}\right) \times 100\ \%$$

(1)

Hemolysis rate exceeding 5% is considered hemolysis.

2.2.5. Effects of PLGA nanoparticles on APTT, PT, TT and Fbg

The blood was collected from healthy rabbits, mixed with sodium citrate in a 9:1 ratio to prevent coagulation. Briefly method, the mixture was centrifuged at 3000 rpm for 10 minutes, then the top supernatant was collected as platelet-poor-plasma (PPP). The solution (10 μL) was incubated with PPP (300 μL) at 37 °C for 30 min. Finally, the incubated mixture was conducted evaluation of effects of nanoparticles on plasma coagulation include activated partial thromboplastin time (APTT), prothrombin time (PT), thrombin time (TT), and fibrinogen (Fbg) levels using a fully automated coagulation apparatus.

2.2.6. Activation of platelet α-granule membrane protein (GMP-140) by PLGA nanoparticles

Rabbit venous blood was anticoagulated with sodium citrate in a ratio of 9:1, centrifuged at 1000 rpm for 10 min, and the supernatant was collected to obtain as platelet-rich plasma (PRP). Then, the PLGA nanoparticles solution (10 μL) was incubated with PRP (300 μL) at 37 °C for 30 min, the incubated mixture was tested with ELISA kit.

2.2.7. Animal experiment

Army Medical University Animal Experiment Ethics Committee and Authority approved all animal procedures for Animal Protection. ApoE$^{-/-}$ and C57 mice were used in this study in accordance with the guidelines of the Chinese Animal Care and Use Committee standards.

The experimental animals were fed with an adaptive feeding week. As shown in Table 1, twenty C57 mice were randomized into two groups, and forty ApoE$^{-/-}$ mice were randomized into four groups (10 mice per group). Then, the mice were subjected to the different treatments for 12 weeks. PLGA nanoparticles was injected at a dose of 10 mg/kg and the frequency of injection was once every two days. The control group was injected with an equal volume of 5% glucose isotonic solution. During the experiment, all the experimental animals were fed with high-fat diet, freely drinking water.

After treatment for 12 weeks the serum, from the mice were harvested. Total cholesterol (TC), triglyceride (TG), high density lipoprotein (HDL-C) and low-density lipoprotein (LDL-C) were detected using an automated biochemical analyzer.

Table 1
Group of experimental animals

Strain	Processing method	Name	Injection frequency	Injection dose	Quantity
C57	12w-Glu	C57	2 days / time	150 μl	10
C57	12w-PLGA	C57 + NPs	2 days / time	10 mg/kg	10
ApoE$^{-/-}$	12w-Glu	ApoE$^{-/-}$(L)	2 days / time	150 μl	10
ApoE$^{-/-}$	12w-PLGA	ApoE$^{-/-}$+NPs(L)	2 days / time	10 mg/kg	10
ApoE$^{-/-}$	8w-HFD + 4w-Glu	ApoE$^{-/-}$(S)	2 days / time	150 μl	10
ApoE$^{-/-}$	8w-HFD + 4w-PLGA	ApoE$^{-/-}$ +NPs(S)	2 days / time	10 mg/kg	10

2.2.8. Analysis of Atherosclerotic Plaques

ORO staining of the cross-sections of the aortic roots was performed as previously described [33]. After treatment for 12 weeks the aortas, from the heart to the iliac bifurcation, from the mice were harvested. Aortas were fixed by perfusion with paraformaldehyde (4% in PBS). After removing the periadventitial tissue, aortas were dissected longitudinally, and then stained with oil red O (ORO) to quantify the plaque area. The extent of atherosclerotic plaque at the aortic root was also determined by ORO staining.

2.2.9. Histology and Immunohistochemistry Staining of the Aortic Root

Histology and Immunofluorescence staining of the cross-sections of the aortic roots was performed as previously described [33]. The aortic roots were fixed with paraformaldehyde (4% in PBS) for 1 h, and then prepared to paraffin sections. After dewaxing, Masson's trichrome and Hematoxylin and eosin (H&E) staining were used to observe the collagen, lipid core and some plaque ruptures. For immunohistochemistry analysis, the activity of the endogenous peroxidase was inhibited by immersion into 3% hydrogen peroxide and 100% methanol for 20 min. Then, the sections were blocked with 5% bovine serum albumin in PBS for 60 min. Antibodies to TNF-α, IL-6, IL-10. Sections of the main organs including heart, liver, spleen, lung, and kidney were also analyzed by H&E staining.

2.2.10. PLGA nanoparticles co-localization with the inflammatory plaque site

DiI@PLGA nanoparticles solution (2 mg/mL) was prepared by the similar preparation method of PLGA nanoparticles described in previous part, mixing DiI solution (1 mM, 15 μL) and PLGA (15 mg) dissolved in 1 mL DMSO. Then the DMSO is removed.The volume was adjusted to 7.5 ml to obtain 2 mg/ml DiI@PLGA nanoparticles solution. C57 mice were control group, and $ApoE^{-/-}$ mice were experimental group (3 mice per group). The experimental animals were fed with HFD for 12 weeks, then DiI@PLGA (200 μL) was injected through the tail vein. After 24 h, mice were euthanized, perfused with PBS containing 4% paraformaldehyde and heparin sodium, and the heart was isolated. Immunofluorescence staining of the cross-sections of the aortic roots was performed as previously described [33]. The frozen sections of carotid roots were incubated with 5% serum. Then, the sections were incubated with anti-CD68 and CD11b antibody overnight at 4 °C, followed by Donkey anti-rabbit IgG H&L for 2 h at room temperature. Samples were stained with DAPI to show the cell nucleus. The sections were observed by the confocal laser scanning microscopy (SP8, Leica, Germany).

2.2.11. PLGA nanoparticles co-culture with Raw264.7 cells

Raw 264.7 cells were cultured in DMEM medium containing 10% fetal bovine serum (FBS) at 37 °C with 5% CO_2. After 6 h incubation, the first medium was discarded. The cells were starved for 12 h, then treated with different concentrations (0, 50, 100, 200, 400 μg/mL) of PLGA nanoparticles and PLGA + PC, and added DMEM without serum. After incubating in a 37 ℃ 5% CO_2 incubator for different times (4, 12, 24, and 48 h), 20 μL of MTS assay solution was added to each well, and incubation was continued for 1 h. The absorbance (OD) of each well was measured at a wavelength of 490 nm using a microplate reader, and repeated six times at each time point. Cell viability was obtained by the following equation:

Cell viability = (ODT - ODB) / (ODC - ODB) × 100% (2)

ODT indicates the absorbance of the experimental group; ODC indicates the absorbance of the control group; and ODB indicates the blank absorbance.

2.2.12. PLGA nanoparticles phagocytized by Raw264.7 cells

Raw264.7 cells were seeded in 12-well plates at a density of 2×10^5 cells per well in 1 mL of DMEM medium containing 10% FBS, and cultured at 37 °C with 5% CO_2 for 24 h. 100 μg of DiI@PLGA and DiI@PLGA + PC were added. After incubation for different times (0.5, 2 and 4 h), the cells were washed with PBS, and fixed with paraformaldehyde (4% in PBS). The nuclei of the cells were stained with DAPI. The cells were observed using the confocal laser scanning microscopy (CLSM).

The same experiment of Raw264.7 cells were also carried out in 6-well plates, for the quantitative analysis of PLGA nanoparticles engulfment by flow cytometry.

2.2.13. Effect of PLGA Nanoparticles on the Transformation of Macrophages to Foam Cells

Raw264.7 cells were seeded in 6-well plates at a density of 2×10^5 cells per well in 1 mL of DMEM medium containing 10% FBS, and cultured at 37 °C with 5% CO_2 for 24 h. Different concentrations (0, 50, 100, 200, 400, 500 μg/mL) of PLGA nanoparticles and PLGA + PC were used to treat Raw264.7 cells simulated with ox-LDL (50 mg/L). After incubation for 48 h, ORO staining was performed of the treated Raw264.7 cells, then observed and photographed using a microscope. Other treated Raw264.7 cells were collected by trypsinization centrifuged at 1000 rpm for 10 min, ultrasonic crushing 1 min. Total cholesterol (TC) and free cholesterol (FC) were measured according to the TC kit and FC kit methods, and the protein content was determined according to the BCA kit method. The content of various cholesterol in Raw264.7 cells was expressed by TC and FC per gram of cellular protein. Each experiment was repeated 3 times [34].

3. Results

3.1. Characterization and blood compatibility of PLGA nanoparticles

The DLS results showed that the diameters of PLGA and PLGA + PC in the water phase were 92.7 ± 3.1 nm and 123.8 ± 5.3 nm, respectively. The Zeta potentials were − 31.6 ± 2.8 mV and − 12.0 ± 3.5 mV, respectively (Fig. 1C and D). PLGA + PC particles in an aqueous solution were larger than PLGA nanoparticles alone and were less stable. Under dry conditions, TEM (Fig. 1Aand B) showed that PLGA and PLGA + PC were spherical particles consistent in size with the DLS measurements. Serum protein concentrations, measured by a bicinchoninic acid (BCA) protein assay, decreased after incubation and confirmed the presence of a protein corona on the PLGA nanoparticles due to the formation of PLGA + PC (Fig. 1E).

As shown in Fig. 1F, the hemolysis rates of 1 mg/ml PLGA nanoparticles, 2 mg/ml PLGA nanoparticles, and PLGA + Glu were 2.96 ± 0.10%, 3.24 ± 0.14%, and 2.95 ± 0.29%, respectively. Hemolysis rates in three experimental groups were less than 5%, according to the national standard for the hemolysis rate of medical biological materials. There were no significant differences in GMP-140, APTT, PT, TT and Fbg values between the negative control group and the experimental groups, indicating that PLGA nanoparticles had no significant effect on coagulation and did not induce platelet activation (Fig. 1G and H).

3.2. PLGA nanoparticles promote the development of atherosclerotic lesions in ApoE$^{-/-}$ mice

The *in vivo* effects of PLGA nanoparticles on the development of atherosclerotic lesions were investigated by continuous PLGA nanoparticle injection and administration of a HFD to ApoE$^{-/-}$ mice. Atherosclerotic plaque formation was detected in the aortic sinus, with a large number of red fat granules accumulating in the ApoE$^{-/-}$ mice groups compared to the C57 control groups (Fig. 2A). The areas of plaque and lipid deposition were severe in each PLGA nanoparticle injection group, 23.24 ± 0.8% vs. 16.99 ± 1.8%, 22.03 ± 1.4% vs. 16.95 ± 1.1% (Fig. 2D). These results suggest that the combination of PLGA nanoparticles and HFD promote the formation of atherosclerotic plaques in ApoE$^{-/-}$ mice.

Next, we examined the composition of atherosclerotic plaques in aortic root sections by immunohistochemistry staining. Hematoxylin and eosin (H&E) staining of aortic sinuses in ApoE$^{-/-}$ mice revealed extensive plaque formation and severe stenosis in the lumen (Fig. 2B). Thickening of the intima and irregular bulging in the lumen, an increase in cell hyperplasia and atherosclerotic plaque formation below the intima were observed. The structure of the arterial wall was disordered, the media was contracted and atrophied, and ruptured plaques with lipid cores were apparent. The collagen arrangement in the aortic sinuses of each group of ApoE$^{-/-}$ mice was disordered, and collagen fibers in the long-term injection of PLGA nanoparticles group were the most scattered. In addition, blue staining was observed at the edges of the plaques (Fig. 2C).

Hyperlipidemia is known to play an important role in the process of plaque formation. Serum TC, TG, LDL-C and HDL-C were significantly higher in the PLGA nanoparticle groups compared with the HFD ApoE$^{-/-}$ mice group (Fig. 2E). Serum TC in the ApoE$^{-/-}$ mice group was approximately 7-fold higher than in the C57 wild type group; TG was nearly 50-fold higher, and LDL-C and HDL-C were 4-fold higher. However, with the exception of HDL-C, there were no significant differences in other lipid profiles between the HFD and PLGA nanoparticle groups. These observations indicate that PLGA nanoparticles do not cause significant changes in blood serum lipids during the formation of AS in ApoE$^{-/-}$ mice.

3.3. PLGA nanoparticle co-localization within the inflammatory plaque site

Atherosclerosis is characterized by plaque formation and chronic inflammation of the arterial wall. We detected co-localization of PLGA nanoparticles at sites of inflammation by immunofluorescence staining. DiI@PLGA nanoparticles were detected in arterial plaque 24 h after injection into the blood stream. CD68 is a marker for a wide range of macrophages that can effectively label monocytes and macrophages (Fig. 3A). CD11b can label neutrophils, monocytes, and macrophages, and function in adhesion and signal transduction during the inflammatory response (Fig. 3B). The results showed that the PLGA nanoparticles co-localized in the plaque sites with CD68 and CD11b positive cells, indicating that the PLGA nanoparticles had a close relationship with AS inflammation, especially the macrophages. We speculate that the nanoparticles co-localized in the plaque sites because they were detected as foreign objects that stimulated macrophages, causing an inflammatory reaction, and increasing phagocytosis inside the plaque.

3.4. PLGA nanoparticles cause inflammatory factor release

After confirming that PLGA nanoparticles co-localized with inflammatory cells in atherosclerotic plaques, we investigated the effects of PLGA nanoparticle injection on the expression of the inflammatory factors TNF-α, IL-6 and IL-10 (Fig. 4A). Positive expression of TNF-α and IL-6 was indicated by brown particles located mainly in the cytoplasm of endothelial and smooth muscle cells. Expression was pronounced in the plaques of the 12-week PLGA nanoparticle injection groups as indicated by dark brown staining. The expression of IL-10 was strongly positive at plaque sites in the $ApoE^{-/-}$ mice groups compared with that in the C57 mice groups, but no significant differences were found between each PLGA nanoparticle injection group and their respective controls (Fig. 4B). These observations indicate that under the influence of a HFD, continuous long-term injection of PLGA nanoparticles can promote an inflammatory response in the plaques of $ApoE^{-/-}$ mice, and PLGA nanoparticles coupled with a HFD had a long-term synergistic effect on the production of AS lesions.

3.5. PLGA nanoparticles were phagocytized by macrophages and decreased cell viability

Macrophages are key contributors to the atherosclerotic process due to their inflammatory and phagocytosis inducing properties. The dynamic phagocytosis of nanoparticles by macrophages was investigated using DiI loaded nanoparticles and observed under confocal laser scanning microscopy (CLSM) and flow cytometry. Raw 264.7 cells began to phagocytize PLGA nanoparticles and PLGA + PC from 0.5 h and increased over time (Fig. 5A, B and C). The red fluorescence in the PLGA + PC group was more evident in the nucleus compared to the PLGA nanoparticle group. Presumably, the protein corona on the PLGA nanoparticle surface was more likely to help the nanoparticles enter the nucleus (Fig. 5A). The amount of phagocytosis after treatment with nanoparticles for 0.5 h by DiI@PLGA and DiI@PLGA + PC was 35.8% and 2.57%, respectively; after 2 h, phagocytosis increased to 88.2% and 7.72%, respectively; then increased to 92.0% and 22.9% after 4 h, respectively (Fig. 5B and C).

To confirm whether the accumulated PLGA nanoparticles would be phagocytized by macrophages and influence their function, we conducted cell viability assays of Raw 264.7 macrophages co-cultured with different PLGA nanoparticle concentrations. The activity of Raw 264.7 cells decreased but remained greater than 60% using different concentrations of PLGA nanoparticles and PLGA + PC treated cells (Fig. 5A and B). When the concentration was less than 100 μg/ml, we observed no significant effects on the viability of Raw 264.7 cells. However, when the concentration was greater than 200 μg/ml, the viability of Raw 264.7 cells decreased significantly at all-time points except 4 h. These observations indicated that PLGA nanoparticles and PLGA + PC affect Raw 264.7 cell viability in a time and dose-dependent manner.

3.6. PLGA nanoparticles promote macrophage transformation to foam cells

One of the typical pathological hallmarks of atherosclerosis is the excessive accumulation of ox-LDL and cholesteryl esters in macrophages and their conversion to foam cells. After accumulating in atherosclerotic plagues, PLGA nanoparticles phagocytized by macrophages will influence the formation of foam cells. To investigate the effects of PLGA nanoparticles and PLGA + PC on macrophage transformation to foam cells, we first treated Raw 264.7 cells with 50 μg/mL ox-LDL and then treated the cells with PLGA nanoparticles or PLGA + PC at different concentrations (0, 50, 100, 200, 400, 500 μg/mL) for 48 h. PLGA nanoparticles and PLGA + PC both promoted the phagocytosis of ox-LDL by Raw 264.7 cells, and reached a maximum at 400 μg/ml. The phagocytosis of ox-LDL by Raw 264.7 cells decreased when the nanoparticle concentration was 500 μg/mL compared with 400 μg/mL, probably because the phagocytosis of ox-LDL had reached saturation and nanoparticles could no longer produce an effect. Compared with PLGA nanoparticles, PLGA + PC more strongly promoted the phagocytosis of ox-LDL into Raw 264.7 cells at the same concentration (Fig. 6A and B). Nanoparticles also increased the Raw 264.7 CE/TC values (%) at higher concentrations but showed no significant differences at concentrations less than 100 μg/mL (Fig. 6C). These findings confirmed that PLGA nanoparticles and PLGA + PC will accelerate the transformation of Raw 264.7 macrophages into foam cells, and that PLGA + PC has a stronger effect than PLGA nanoparticles.

4. Discussion

Due to their unique physico-chemical characteristics, advantages of NPs in this context include their ability to easily penetrate across cell barriers, preferential accumulation in specific orga-nelles and cells, and theranostic (both therapy and diagnostic) properties, as well as their capacity for fine tuning. Polymer nanoparticles are attracting attention due to high efficiency, long-term circulation characteristics, and metabolic discharge mechanisms that are superior to other biomaterials. These beneficial properties have resulted in the widespread use of polymer nanoparticles as drug delivery systems and diagnostic contrast agents for medical applications. Despite their good biocompatibility, there are also disadvantages of polymer biomaterials in nano scale, especially under pathological conditions and the interactions of NPs

with living cells are complex and still far from fully understood [35].This article focuses on polymer nanoparticles and explores their impact on the development of cardiovascular diseases such as AS and possible mechanisms of function.

Current research has shown that nanoparticles < 100 nm in size are easily absorbed by tissues [36]. PLGA nanoparticles prepared by dialysis were characterized by DLS and TEM and found to possess the expected size (nanoscale) and useful characteristics such as good dispersion, uniform size and spherical shape. In addition to the standard physical criteria, medical biomaterials must also exhibit a high degree of compatibility with the circulatory system. Therefore, we evaluated blood compatibility of PLGA nanoparticles from three aspects, hemolysis rate and coagulation function and platelet activation. The hemolysis rate of PLGA nanoparticles was < 5%, in accordance with international standards. The physiological anticoagulant function is mainly achieved through the joint action of the coagulation system, platelets and the fibrinolysis system [37]. APTT mainly reflects the activity and function of endogenous coagulation factors, PT represents the exogenous coagulation system, TT is the time for conversion of fibrinogen to fibrin, Fbg is the content of fibrinogen, and GMP-140 indicates the activation of platelets. Through the detection of these five indicators, we found that the prepared PLGA nanoparticles did not have a significant impact on coagulation and had excellent blood compatibility.

In 2017, Miller et al. studied the effects of gold nanoparticles on cardiovascular disease, and discovered that red and purple particles accumulated in foam cells at sites of atherosclerotic plaque in $ApoE^{-/-}$ mice treated with gold nanoparticles [38]. Furthermore, gold nanoparticles could be detected in surgical specimens of carotid artery disease from patients at risk of stroke. Based on previous research, in this paper we investigated the effects of PLGA nanoparticles on atherosclerosis by administrating PLGA nanoparticles to $ApoE^{-/-}$ mice by intravenous injection. The $ApoE^{-/-}$ mice were fed a HFD and injected with PLGA nanoparticles for 12 weeks to investigate the effects of nanoparticles on the development of atherosclerosis. In a second experimental group, $ApoE^{-/-}$ mice were fed a HFD for 8 weeks to form atherosclerotic plaques, then PLGA nanoparticles were injected simultaneously for 4 weeks. Wild type C57 mice were used as a healthy vascular control group. We observed that PLGA nanoparticles caused a significant increase in plaque area and accumulated in the inflammatory sites during 4 weeks and 12 weeks of injection. In addition, PLGA nanoparticles promoted the activation of macrophages, secreting a large number of inflammatory factors, at sites of plaque formation. These inflammatory factors, which include the matrix metalloproteinases, are the major proteins that regulate the activity of inflammatory cells. Matrix metalloproteinases degrade the extracellular matrix and reduce the collagen and elastin content in the plaque lipid core. In the presence of atherosclerotic lesions, PLGA nanoparticles promote these pathological phenomena.

In wild-type C57 mice with no plaque formation, immuno-histochemical staining detected only small amounts of the pro-inflammatory factors TNF-α and IL-6 on the blood vessel walls and no expression of the anti-inflammatory factor IL-10. These observations indicated that in the absence of AS lesions (i.e., under normal physiological conditions) in mice, there was no significant inflammation and inflammatory

factors were not activated and released. In the ApoE$^{-/-}$ mice group that could spontaneously form AS plaques, strong positive expression of the pro-inflammatory cytokines TNF-α and IL-6 could be clearly observed at plaque sites. After 12 weeks of injection of PLGA nanoparticles, TNF-α and IL-6 levels increased significantly compared to the control groups. At the same time, IL-10 anti-inflammatory factors also showed strong positive expression. Therefore, during the process of AS plaque formation, PLGA nanoparticles aggravate inflammatory reactions and anti-inflammatory protective effects, causing increased secretion and release of pro-inflammatory factors such as TNF-α and IL-6 and anti-inflammatory factors such as IL-10 to avoid serious tissue damage. These results were consistent with recent studies regarding the relationships between inflammation and anti-inflammatory factors such as TNF-α/IL-10. Internal environmental stability is based on the dynamic balance between inflammatory and anti-inflammatory responses. When the inflammatory response dominates, tissues and cells will be damaged; whereas, a strong anti-inflammatory reaction will inhibit immune function [39]. We initially determined that PLGA nanoparticles enter the body as foreign objects, triggering an inflammatory response in ApoE$^{-/-}$ mice. These nanoparticles were then engulfed by macrophages, migrated to sites of inflammation and eventually aggravated the formation of plaque.

During the injection process, nanoparticles are rapidly coated with macromolecules forming a "protein crown or corona (PC)", which alters the size, aggregation state, surface charge and interfacial properties of the nanomaterials to create a biological identity that is distinct from its original synthetic identity. PLGA nanoparticles adsorbed a certain amount of proteins to form the PLGA + PC, with larger diameter and less stability, after incubation with mouse serum. Nanoparticles with protein coronas show completely different cell recognition or biological effects *in vitro* compared with *in vivo* [30].

Macrophages are the most important inflammatory cells in the process of AS lesion formation, are important components of lipid plaques, and serve as an important source of foam cells [40]. Therefore, we studied the effects of PLGA nanoparticles on macrophages *in vitro*. According to the MTS assay results, the activity of Raw 264.7 cells decreased with increasing concentrations of PLGA nanoparticles and PLGA + PC. The presence of the protein corona inhibited the phagocytosis of PLGA nanoparticles by Raw 264.7 cells. Studies have shown that the role of the protein corona in biological systems can be divided into "opsonins" and "dysopsonins" [41]. Opsonins promote macrophage phagocytosis, while dysopsonins inhibit phagocytosis. The structure and composition of the corona depend on the synthetic identity of the nanomaterial, which includes the chemistry, topography and curvature of the nanomaterial. Polymer nanoparticles possess various chemical compositions, free residues and morphologies (such as spheres, rods, vesicles, tubules and lamellae), which provide them with more diverse synthetic identities. After PLGA nanoparticles enter the blood stream, the surface-adsorbed dysopsonins may be more abundant and more stable.

The physiological functions of proteins that comprise the protein corona include lipid transport, blood coagulation, complement activation, pathogen recognition and ion transport [42]. In the early stages of AS, ox-LDL acts as an inflammatory medium, promoting foam cell development and cholesterol-rich lipid

core formation [43]. Cell ORO staining and CE/TC% suggested that PLGA nanoparticles and PLGA + PC accelerated the conversion of Raw 264.7 cells to foam cells and that PLGA + PC had a stronger effect than PLGA nanoparticles. Therefore, the protein corona absorbed on the surface of PLGA nanoparticles may possess a stronger atherogenic potential. This phenomenon may explain many existing inconsistencies between *in vitro* toxicity screening and *in vivo* studies, and necessitate a re-evaluation of the toxicity of polymer nanoparticles, even for polymer materials with good biocompatibility.

5. Conclusion

In this study, we observed that phagocytosis of polymeric nanoparticles with good blood compatibility may promote the formation of atherosclerotic plaques and development of cardiovascular risk factors such as dyslipidemia, inflammation, and abnormal hemodynamics. These adverse cardiovascular effects may result from macrophage activation and transformation into foam cells, followed by an increase in inflammatory factors. The types of proteins and amount of protein corona absorbed on the surface of polymeric nanoparticles may play a key role during this process. These *in vivo* results highlight the neglected hazard for polymeric nanoparticles what we should consider in future nanomaterial design and pay more attention to the process of using nano-medicines on cardiovascular diseases.

Declarations

Funding

This research was supported by the National Natural Science Foundation of China (12032007, 31971242); the Natural Science Foundation of Chongqing (cstc2019jcyj-msxmX0307, cstc2019jcyj-19zdxmX0009, cstc2019jcyj-zdxmX0028); the Fundamental Research Funds for the Central Universities (2019CDYGZD002, 2020CDCGJ011). The author would like to thank all other members of Professor Guixue Wang's laboratory (Chongqing Engineering Laboratory in Vascular Implants and the Public Experiment Center of State Bioindustrial Base (Chongqing)) for their daily experimental and management work.

Availability of data and materials

The datasets used and analysed during the current study are available from

the corresponding author on reasonable request.

Ethics approval and consent to participate

Army Medical University Animal Experiment Ethics Committee and Authority approved all animal procedures for Animal Protection. The manuscript does not contain clinical studies or

patient data.

Competing interests

The authors declared that they have no conflicts of interest.

Author details

[1] Key Laboratory for Biorheological Science and Technology of Ministry of Education, State and Local Joint Engineering Laboratory for Vascular Implants, Bioengineering College of Chongqing University, Chongqing, 400044, China

[2] School of medicine, Chongqing University, Chongqing, 400030, China

* Corresponding author. Bioengineering College of Chongqing University, Chongqing, 400044, China

E-mail addresses: tieying_yin@cqu.edu.cn (T.Y. Yin), wanggx@cqu.edu.cn (G.X. Wang), yazhou_wang@cqu.edu.cn (Y.Z. Wang)

Fax: 86(0)23-6510 0026

Telephone Number: 86(0)23-6510 0090

References

1. Mahmoudi M, Yu M, Serpooshan V, Wu JC, Langer R, Lee RT, Karp JM, Farokhzad OC. Multiscale technologies for treatment of ischemic cardiomyopathy, Nanotechnol. 2017;12:845-855.
2. Cheng CT, Castro G, Liu CH, Lau P. Advanced nanotechnology: An arsenal to enhance immunotherapy in fighting cancer, Chim. Acta. 2019;49:12-19.
3. Yu XH., Hong FS., Zhang YQ. Bio-effect of nanoparticles in the cardiovascular system, J. Mater. Res. A. 2016;104:2881-2897.
4. Gonzalez C, Rosas-Hernandez H, Lee MAR, Salazar-García S, Ali SF. Role of silver nanoparticles (AgNPs) on the cardiovascular system, Arch. Toxicol. 2016;90:493-511.
5. Wang YZ, Wang GX. Polymeric nanomicelles: a potential hazard for the cardiovascular system? Nanomedicine (Lond). 2017;12:1355-1358
6. Feng L, Yang XZ, Shi YF, Liang S, Zhao T, Duan JC, Sun ZW. Co-exposure subacute toxicity of silica nanoparticles and lead acetate on cardiovascular system, Int. J. Nanomedicine. 2018;13:7819-7834.
7. Yang Y, Du ZJ, Liu XM. Experimental research advances in toxic effects of silica nanoparticles on cardiovascular system, Zhonghua. Lao. Dong. Wei. Sheng. Zhi. Ye. Bing. Za. Zhi. 2018;36: 711-713.
8. Zhou T, Dong QL, Shen Y, Wu W, Wu HD, Luo XL, Liao XL, Wang GX. PEG- b-PCL polymeric nano-micelle inhibits vascular angiogenesis by activating p53-dependent apoptosis in zebrafish. International Journal of Nanomedicine. 2016;11:6517-6531.

9. Stoupel EG. Cosmic ray (neutron) activity and air pollution nanoparticles - cardiovascular disease risk factors - separate or together? J. Basic. Clin. Physiol. Pharmacol. 2016;27:493-496.
10. Lee HC, Lin TH. Air pollution particular matter and atherosclerosis, Acta. Cardiol. Sin. 2017;33:646-647.
11. Bostan HB, Rezaee R, Valokala MG, Tsarouhas K, Golokhvast K, Tsatsakis AM, Karimi G. Cardiotoxicity of nano-particles, Life Sci. 2016;165:91-99.
12. Yu X, Hong F, Zhang YQ. Bio-effect of nanoparticles in the cardiovascular system, Biomed. Mater. Res. A. 2016;104:2881–2897.
13. Hou ZJ, Yan WH, Li TH, Wei W, Cui YL, Zhang XJ, Chen YP, Yin TY, Qiu JH, Wang GX. Lactic acid-mediated endothelial to mesenchymal transition through TGF-β1 contributes to in-stent stenosis in poly-L-lactic acid stent. Int J Biol Macromol. 2020;155:1589-1598.
14. Tian L, Lin B, Wu L, Li K, Liu H, Yan J, Liu X, Xi Z. Neurotoxicity induced by zinc oxide nanoparticles: age-related differences and interaction, Sci. Rep. 2015;5:16117.
15. Duan J, Hu H, Li QL, Jiang LZ, Zou Y, Wang Y, Sun ZW. Combined toxicity of silica nanoparticles and methylmercury on cardiovascular system in zebrafish (Danio rerio) embryos, Environ. Toxicol. Pharmacol. 2016;44:120-127.
16. Haber N, Hirn S, Holzer M, Zuchtriegel G, Rehberg M, Krombach F. Krombach, Effects of acute systemic administration of TiO2, ZnO, SiO2, and Ag nanoparticles on hemodynamics, hemostasis and leukocyte recruitment. Nanotoxicology, 2015;9:963-971.
17. Kim AY, Ha JH, Park SN. Selective release system for anti-oxidative and anti-inflammatory activities using H_2O_2-responsive therapeutic nanoparticles, Biomacromolecules. 2017;18:3197-3206.
18. Reddy ARN, Lonkala S. In vitro evaluation of copper oxide nanoparticle-induced cytotoxicity and oxidative stress using human embryonic kidney cells, Toxicol. Ind. Health. 2019;35:159-164.
19. Guo CX, Xia Y, Niu PY, Jiang LZ, Duan JC, Yu Y, Zhou XQ, Li YB, Sun ZW. Silica nanoparticles induce oxidative stress, inflammation, and endothelial dysfunction in vitro via activation of the MAPK/Nrf_2 pathway and nuclear factor-κB signaling, Int. J. Nanomedicine. 2015;10:1463-1477.
20. Chistiakov DA, Orekhov AN, Bobryshev YV. Bobryshev, Vascular smooth muscle cell in atherosclerosis, Acta. Physiologica. 2015;214:33-50.
21. Bostan HB, Rezaee R, Valokala MG, Tsarouhas K, Golokhvast K, Tsatsakis AM. Gholamreza Karimi Cardiotoxicity of nano-particles, Life. Sci. 2016;165:91-99.
22. Fröhlich E. Value of phagocyte function screening for immunotoxicity of nanoparticles in vivo. Int. J. Nanomedicine. 2015;10:3761-3778.
23. Setyawati MI, Tay CY, Bay BH, Leong DT. Gold nanoparticles induced endothelial leakiness depends on particle size and endothelial cell origin, ACS. Nano. 2017;11:5020-5030.
24. Pillai GJ, Paul-Prasanth B, Nair SV, Menon D. Influence of surface passivation of 2-Methoxyestradiol loaded PLGA nanoparticles on cellular interactions, pharmacokinetics and tumour accumulation, Colloids. Surf. B. Biointerfaces. 2017;150:242-249.

25. Alavi M, Hamidi M. Passive and active targeting in cancer therapy by liposomes and lipid nanoparticles, Drug. Metab. Pers. Ther. 2019;34.
26. Hiroshi M. Toward a full understanding of the EPR effect in primary and metastatic tumors as well as issues related to its heterogeneity, Adv. Drug. Deliv. Rev. 2015;91:3-6.
27. Ahsan SM, Rao CM, Ahmad MF. Nanoparticle-protein interaction: The significance and role of protein corona, Adv. Exp. Med. Biol. 2018;1048:175-198.
28. Jiang WS, Rutherford D, Vuong T, Liu Nanomaterials for treating cardiovascular diseases: A review, Bioact. Mater. 2017;6:185-198.
29. Baimanov D, Cai R. Understanding the chemical nature of nanoparticle-protein interactions, Bioconjug Chem. 2019;30:1923-1937.
30. Ritz S, Schöttler S, Kotman N, Baier G, Musyanovych A, Kuharev J, Landfester K, Schild H, Jahn O, Tenzer S, Mailänder V. Protein corona of nanoparticles: Distinct proteins regulate the cellular uptake, Biomacromolecules, 2015;16:1311-1321.
31. Schwenk JM, Omenn GS. The human plasma proteome draft of 2017: Building on the human plasma peptide atlas from mass spectrometry and complementary assays, J.Proteome.Res. 2017;16:4299-4310.
32. Zhuang J, Fang RH. Preparation of particulate polymeric therapeutics for medical applications, Small. Methods. 2017;1:1700147.
33. Wang Y, Zhang K, Qin X, Li TH, Qiu JH, Yin TY, Huang JL, McGinty S, Pontrelli G, Ren J, Wang QW, Wu W, Wang GX, Biomimetic nanotherapies: Red blood cell based core–shell structured nanocomplexes for atherosclerosis management, Adv Sci (Weinh). 2019;6:1900172.
34. D'Elios MM, Vallese F, Capitani N, Benagiano M, Bernardini ML, Rossi M, Rossi GP, Ferrari M, Baldari CT, Zanotti G, Bernard MD, Codolo G. The Helicobacter cinaedi antigen CAIP participates in atherosclerotic inflammation by promoting the differentiation of macrophages in foam cells, Sci. Rep. 2017;7: 40515.
35. Xu JX, Wang JX, Qiu JH, Liu H, Wang Yi, Cui YL, Humphry R, Wang N, Durkan C, Chen YK, Lu YQ, Ma QF, Wei W, Luo Y, Xiao LH, Wang GX. Nanoparticles retard immune cells recruitment in vivo by inhibiting chemokine expression, Biomaterials. 2021;265:120392
36. Liu P, Chen N, Yan L, Gao F, Ji DS, Zhang SJ, Zhang L, Li YQ, Xiao Y. Preparation of characterisation and in vitro and in vivo evaluation of CD44-targeted chondroitin sulphate-conjugated doxorubicin PLGA nanoparticles, Carbohydr. Polym. 2019;213:17-26.
37. Makarov MS, Borovkova NV, Storozheva MV. Morphofunctional properties of human platelets treated with silver nanoparticles, Bull. Exp. Biol. Med. 2017;164: 241-246.
38. Miller MR, Raftis JB, Langrish JP, McLean SG, Samutrtai P, Connell SP, Wilson S, Vesey AT, Fokkens PHB, Boere AJF, Krystek P, Campbell CJ, Hadoke PWF, Donaldson K, Cassee FR, Newby DE, Duffin R, Mills NL. Inhaled nanoparticles accumulate at sites of vascular disease, ACS. Nano. 2017;11: 4542–4552.

39. Lu J, Sun MS, Wu XJ, Yuan X, Liu Z, Qu XJ, Ji XP, Merriman TR, Li C. Urate-lowering therapy alleviates atherosclerosis inflammatory response factors and neointimal lesions in a mouse model of induced carotid atherosclerosis, Febs. J. 2019;286:1346-1359.
40. Ye J, Guo RW, Shi YK, Qi F, Guo CM, Yang LX. MiR-155 regulated inflammation response by the SOCS1-STAT3-PDCD4 axis in atherogenesis, Mediators. Inflamm. 2016; 8060182.
41. Rezaei G, Daghighi SM, Raoufi M, Esfandyari-Manesh M, Rahimifard M, Mobarakeh VI, Kamalzare S, Ghahremani MH, Atyabi F, Abdollahi M, Rezaee F, Dinarvand R. Synthetic and biological identities of polymeric nanoparticles influencing the cellular delivery: An immunological link, J. Colloid. Interface. Sci. 2019;556:476-491.
42. Walkey CD, Chan WC. Understanding and controlling the interaction of nanomaterials with proteins in a physiological environment, Soc. Rev. 2012;41:2780–2799.
43. Wang Y, Dubland JA, Allahverdian S, Asonye E, Sahin B, Jaw JE, Sin DD, Seidman MA, Leeper NJ, Francis GA. Smooth muscle cells contribute the majority of foam cells in ApoE (Apolipoprotein E)-deficient mouse atherosclerosis, Arterioscler. Thromb.Vasc. Biol. 2019;39: 876-887.

Figures

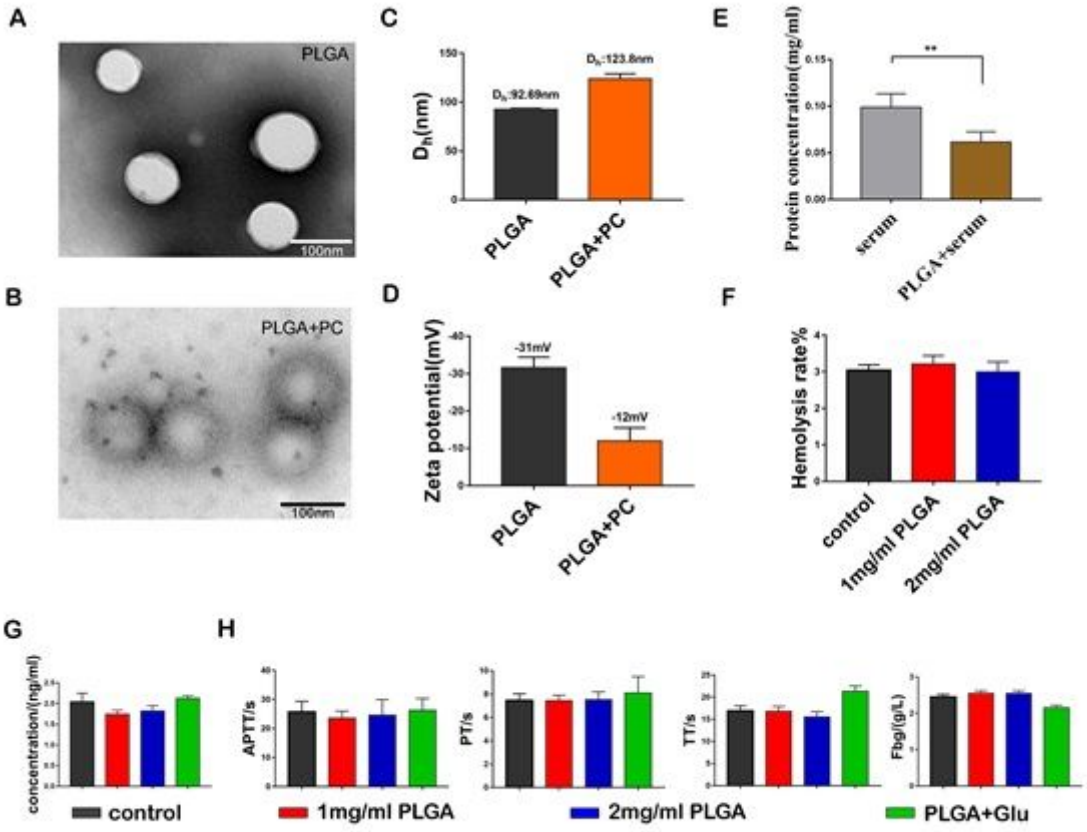

Figure 1

Characterization and blood compatibility of PLGA nanoparticles. TEM morphology of (A) PLGA nanoparticles and (B) PLGA+PC. (C) DLS particle size and (D) electric potential results for PLGA nanoparticles and PLGA+PC. (E) PLGA nanoparticles adsorb proteins in serum to form the protein corona. (F) The hemolysis rate of PLGA nanoparticles. (G) The concentration of α-granule membrane protein in platelets and (H) Response of coagulation variables (APTT, PT, TT, Fbg) after PLGA nanoparticles were added. n = 3, mean ± SD, **P < 0.01.

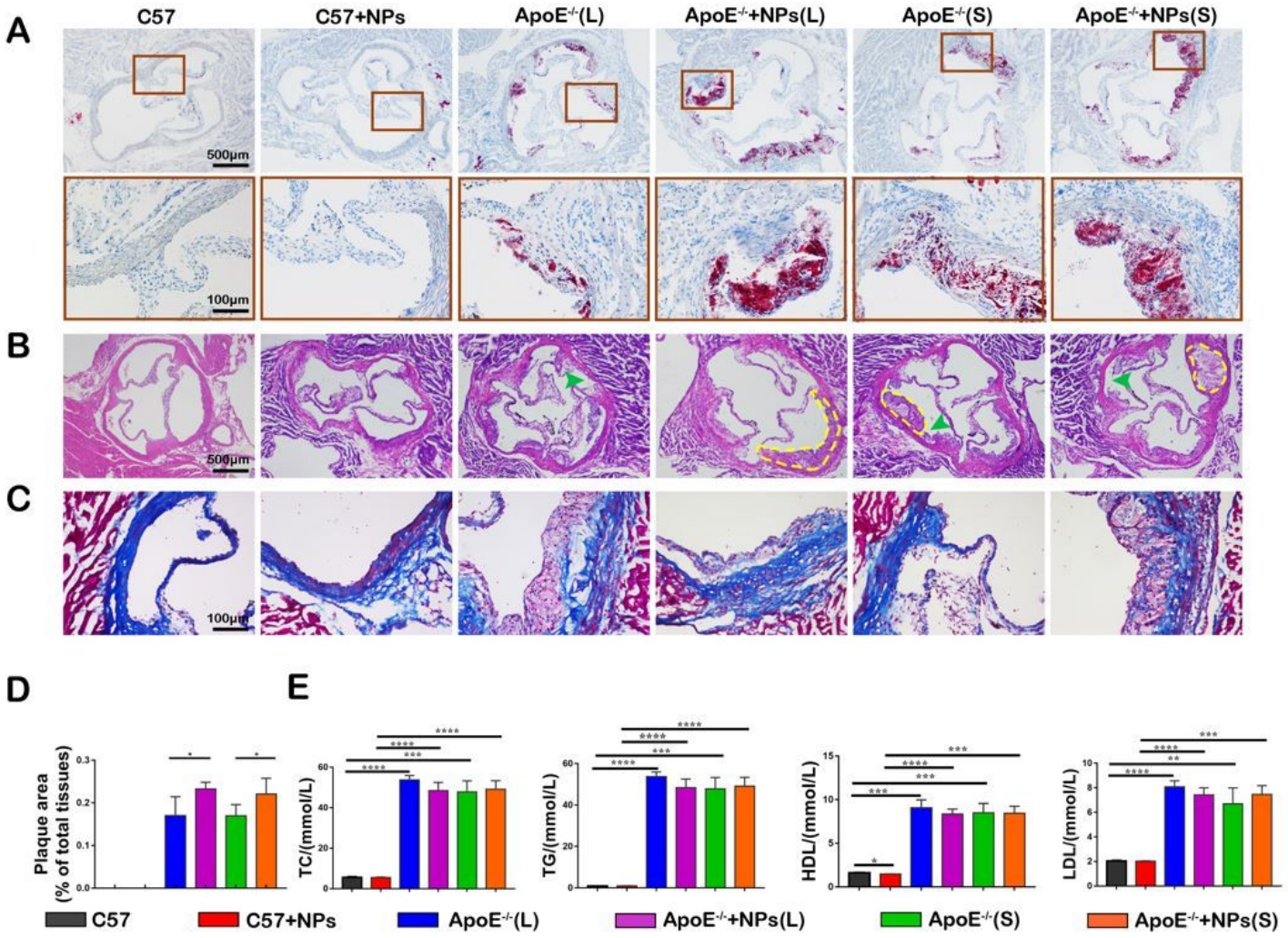

Figure 2

The combination of PLGA nanoparticles and a high-fat diet promotes the formation of atherosclerotic plaques in ApoE-/- mice. (A) ORO stained images of aortic sinus tissues in ApoE-/- and C57 mice. (B) H&E stained images of aortic lipid cores (yellow dashed lineand plaque ruptures (green arrows) in ApoE-/- and C57 mice. (C) Images of collagen in the plaque areas stained by Masson's trichrome. (D) Quantitative data of the atherosclerotic plaque area in the aortic root sections. (E) The lipid assays from serum during atherosclerotic development (TC, TG, LDL, HDL). n = 5, mean ± SD, *P < 0.05; **P < 0.01; ***P < 0.001; ****P < 0.0001.

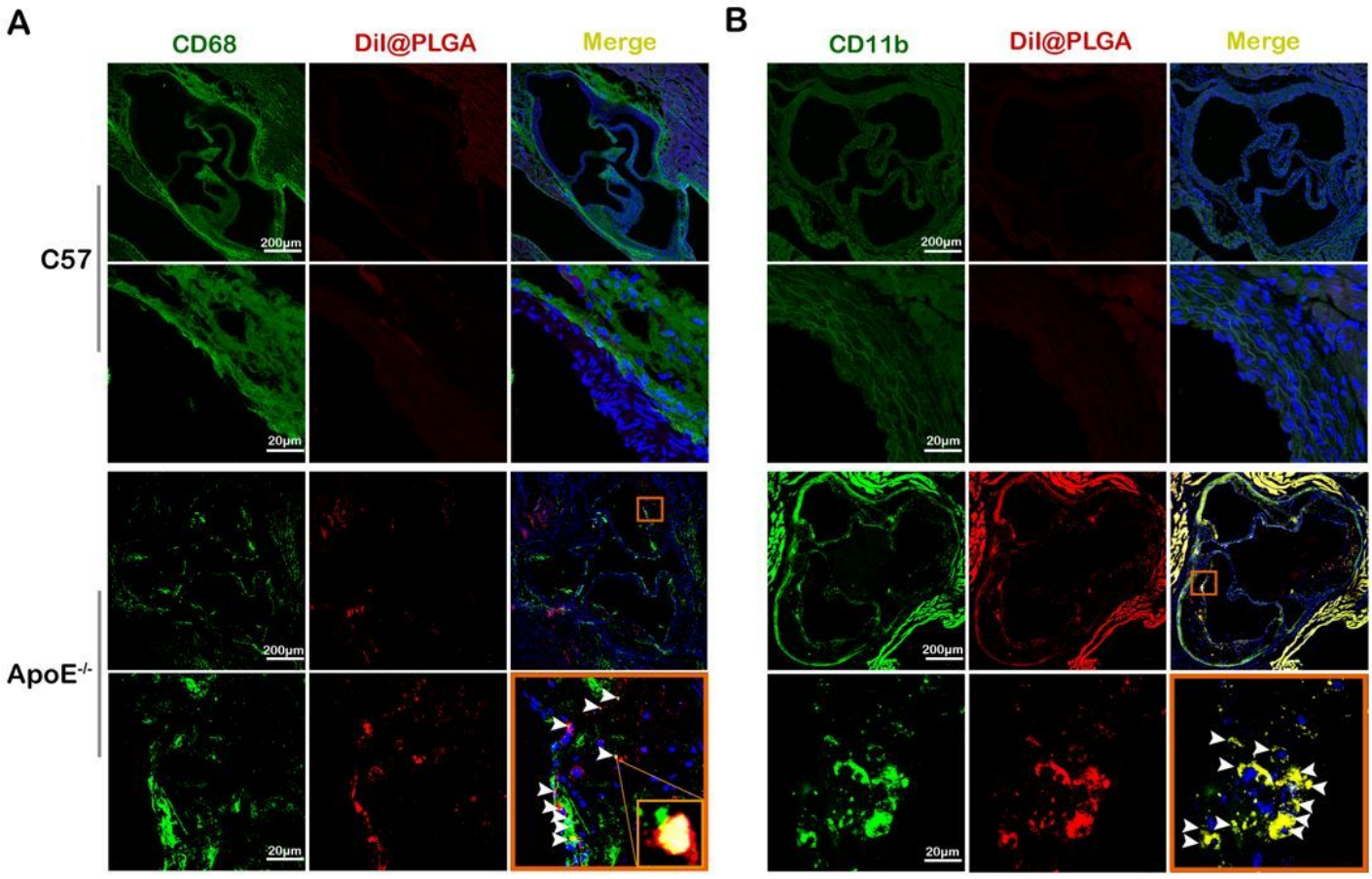

Figure 3

PLGA nanoparticles are enriched at plaque sites (red) and co-localize with inflammatory cells (yellow). The experimental animals were fed with HFD for 12 weeks, then DiI@PLGA (2mg/mL, 200 μL) was injected through the tail vein and DiI@PLGA nanoparticles were detected in arterial plaque 24 h after injection into the blood stream. CLSM images of the PLGA nanoparticles co-localized with (A) CD68 positive cells and (B) CD11b positive cells (white arrow heads).

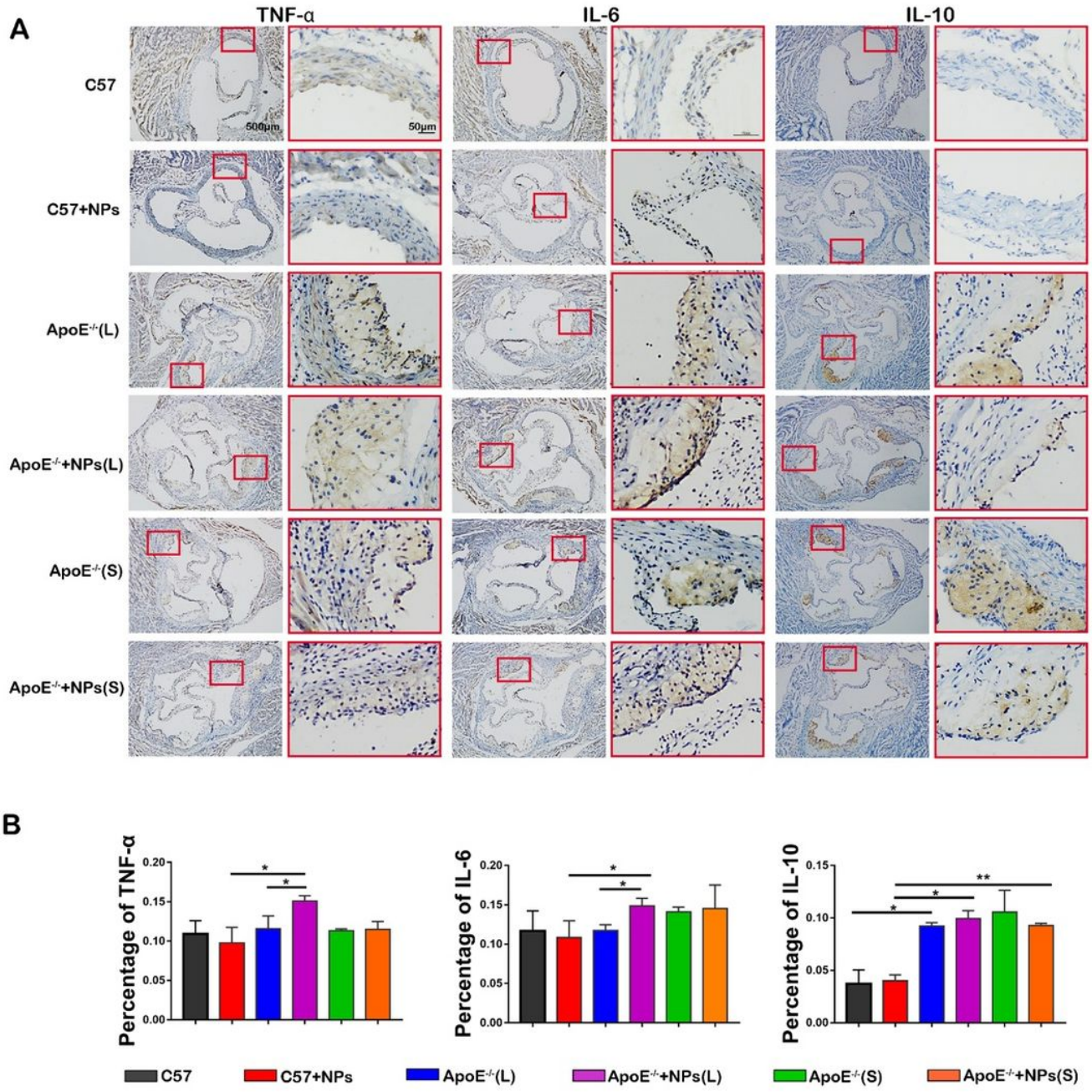

Figure 4

PLGA nanoparticles cause an increasing inflammatory factor release in ApoE-/- mice on a HFD and long-term injection. (A) Representative images of immuno-histochemistry staining with antibodies to TNF-α, IL-6 and IL-10. (B) Quantitative data of TNF-α, IL-6 and IL-10 in plaque areas of the aortic root sections. n = 4, mean ± SD, * P < 0.05; **P< 0.01.

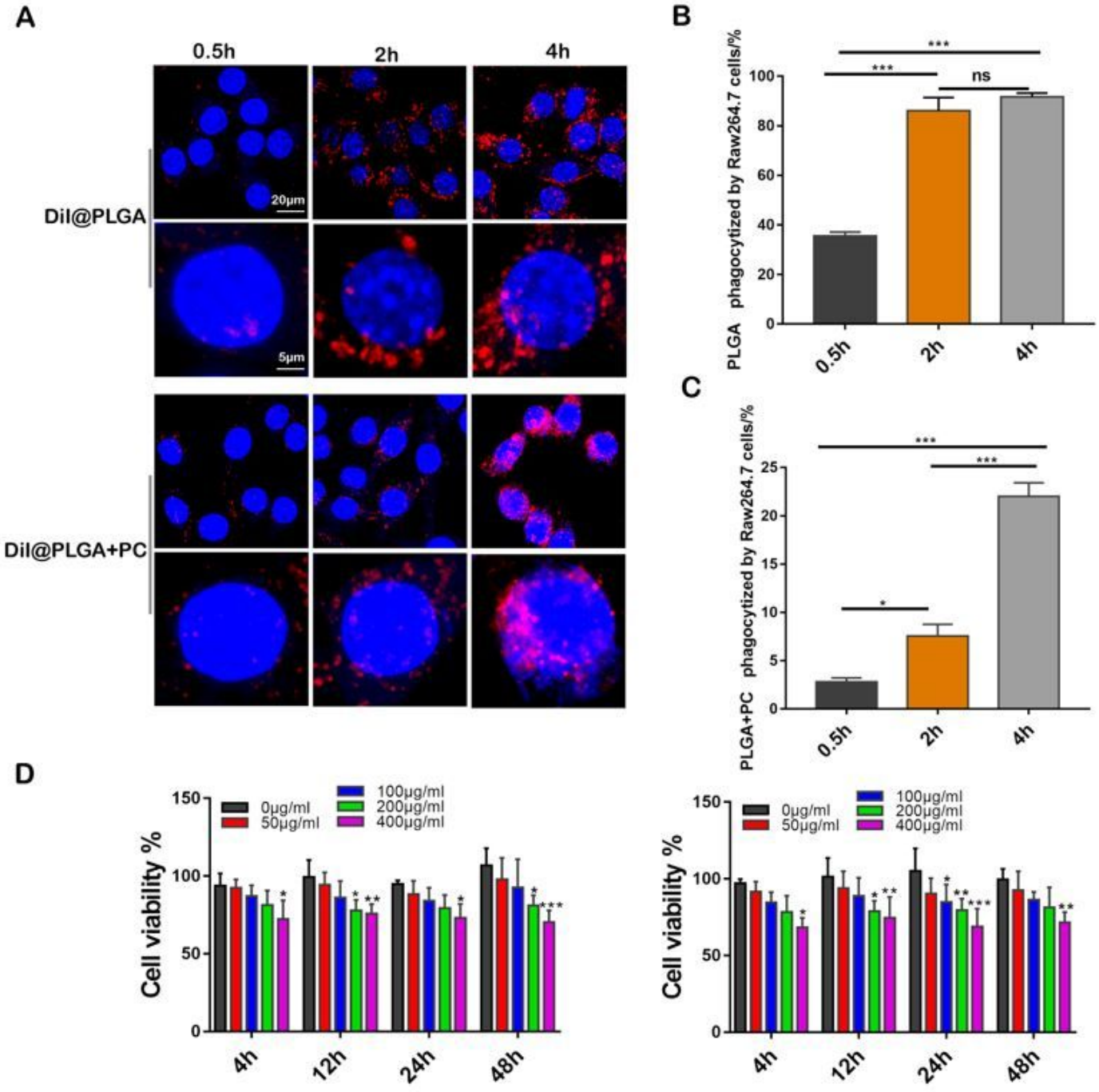

Figure 5

Effects of PLGA nanoparticles and their protein coronas on macrophage activity and phagocytosis. (A) CLSM images of DiI@PLGA and DiI@PLGA+PC phagocytosed by Raw 264.7 macrophages at different time points. Quantification of cellular phagocytosis of (B)DiI@PLGA and (C)DiI@PLGA+PC in Raw 264.7 macrophages at different time points by flow cytometry. (D)Quantitative data of Raw 264.7 macrophage cell viability in different concentrations of PLGA nanoparticles and PLGA+PC. n = 6, mean ± SD, **P < 0.01; ***P< 0.001; ns, not significant.

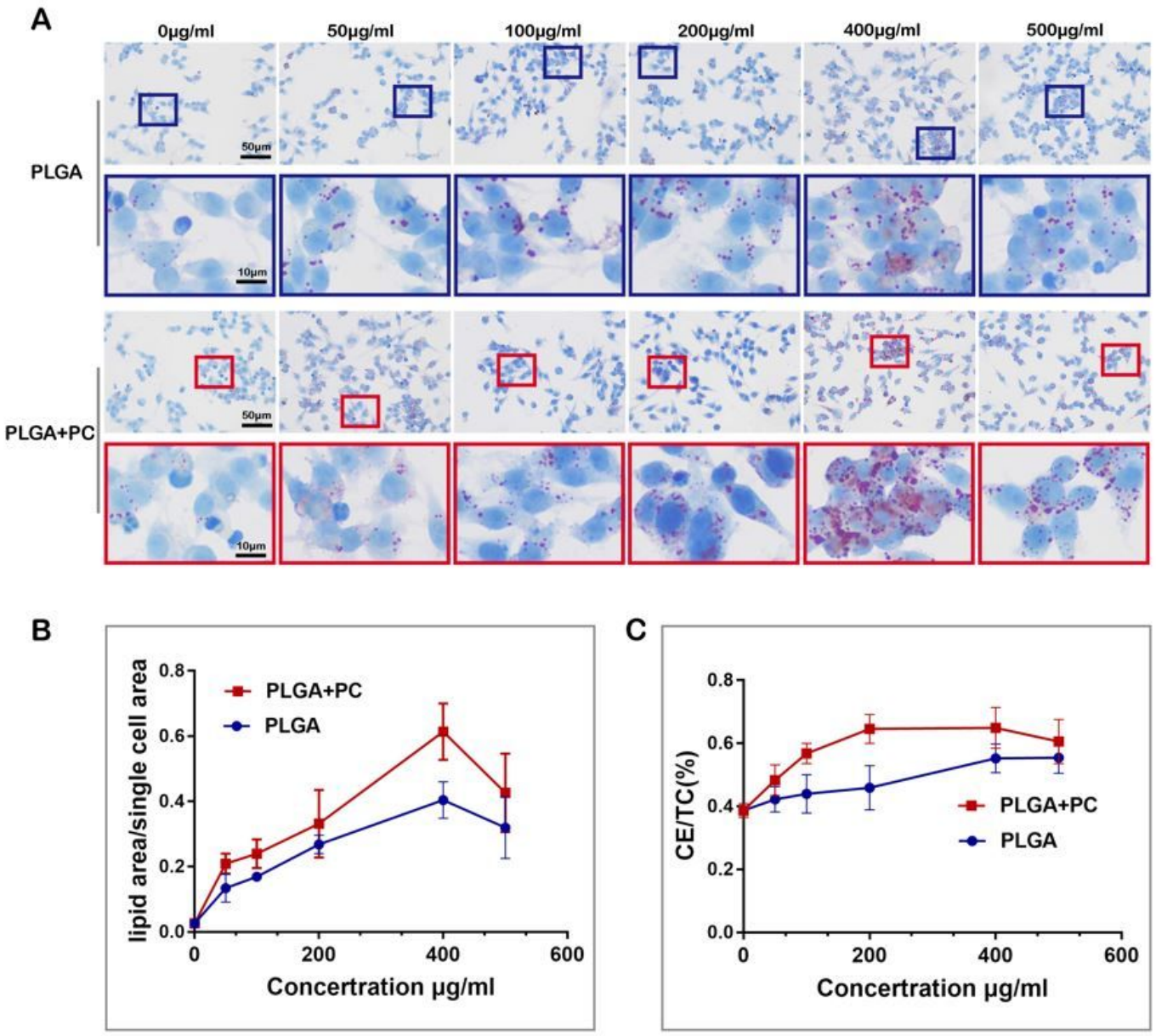

Figure 6

Effects of PLGA nanoparticles and their protein coronas on the transformation of macrophages into foam cells. (A, B) Effects of PLGA nanoparticles and PLGA+PC on the phagocytosis of ox-LDL by Raw 264.7 macrophages. (C) The CE/TC (%) of macrophages to foam cells after treatment with nanoparticles. n = 3, mean ± SD.

Supplementary Files

This is a list of supplementary files associated with this preprint. Click to download.

- Graphicalabstract.pdf